CHEMISTRY OF MATERIALS
Article

Chem. Mater. **2011,** *23,* 155–162 155
DOI:10.1021/cm102389m

Controlled Growth of TiO_2 Nanotubes on Conducting Glass

Jonas Weickert,[†] Claudia Palumbiny,[†] Mihaela Nedelcu,[‡] Thomas Bein,[‡] and Lukas Schmidt-Mende*,[†]

[†]*Ludwig-Maximilians-University Munich, Department of Physics and Center for NanoScience (CeNS), Amalienstrasse 54, D-80809 Munich, and* [‡]*Ludwig-Maximilians-University Munich, Department of Chemistry and Center for NanoScience (CeNS), Butenandtstrasse 5-13, 81377 Munich, Germany*

Received August 19, 2010. Revised Manuscript Received September 30, 2010

We report on nanotubular TiO_2 on top of a compact TiO_2 layer on conducting glass substrates. Highly regular structures were obtained from anodization of DC sputtered Ti films of thicknesses between 0.2 and 2 μm in ammonium fluoride containing ethylene glycol solutions. The influence of different anodization parameters was systematically analyzed revealing that full control over tube length, diameter, spacing, and tube wall thickness is possible. Inner tube diameters and spacing between tubes can be controlled via the anodization field. Tube wall thickness can be tuned using different anodization bath temperatures. Tube length can be adjusted by sputtering appropriate layers of Ti. The resulting TiO_2 structures can be readily used in poly(3-hexylthiophene)-TiO_2 hybrid solar cells and solid state dye sensitized solar cells. In contrast to anodized Ti foils the presented geometry allows the fabrication of photovoltaic devices which can be frontside-illuminated (through the glass substrate).

Introduction

Titania nanotubes have proven to be a highly promising material for application in various fields. Recent publications indicate that nanotubular TiO_2 can be used in sensing,[1] photocatalysis,[2] photoelectrolysis,[3] and photovoltaics.[4]

A suitable method for fabrication of TiO_2 nanotubes is anodization of metallic Ti. Commonly, high purity Ti foils are used and anodized in aqueous HF-containing solutions[5] or NH_4F-containing ethylene glycol electrolytes.[6] Pore sizes and wall thicknesses can be varied for anodized foils,[7] and tube lengths of several hundreds of μm are reported.[8] In contrast, there are only limited studies concerning thin films of anodized Ti sputtered on silicon or conductive glass substrates, and there is no comprehensive study about controlling the above-mentioned parameters in thin films.[9]

However, especially for photovoltaic devices, TiO_2 nanotubes on conducting glass are of particular interest. Thin films of nanostructured TiO_2 would allow cell geometries similar to fully organic bulk heterojunction solar

*Corresponding author e-mail: L.Schmidt-Mende@physik.uni-muenchen.de.

(1) (a) Paulose, M.; Shankar, K.; Varghese, O. K.; Mor, G. K.; Hardin, B.; Grimes, C. A. Backside illuminated dye-sensitized solar cells based on titania nanotube array electrodes. *Nanotechnology* **2006**, *17*(5), 1446–1448. (b) Mor, G. K.; Carvalho, M. A.; Varghese, O. K.; Pishko, M. V.; Grimes, C. A. A room-temperature TiO2-nanotube hydrogen sensor able to self-clean photoactively from environmental contamination. *J. Mater. Res.* **2004**, *19*(2), 628–634. (c) Varghese, O. K.; Gong, D. W.; Paulose, M.; Ong, K. G.; Dickey, E. C.; Grimes, C. A. Extreme changes in the electrical resistance of titania nanotubes with hydrogen exposure. *Adv. Mater.* **2003**, *15*(7−8), 624–627. (d) Mor, G. K.; Varghese, O. K.; Paulose, M.; Ong, K. G.; Grimes, C. A. Fabrication of hydrogen sensors with transparent titanium oxide nanotube-array thin films as sensing elements. *Thin Solid Films* **2006**, *496* (1), 42–48.

(2) (a) Adachi, M.; Murata, Y.; Harada, M.; Yoshikawa, S. Formation of titania nanotubes with high photo-catalytic activity. *Chem. Lett.* **2000**, No. 8, 942–943. (b) Chu, S. Z.; Inoue, S.; Wada, K.; Li, D.; Haneda, H.; Awatsu, S. Highly porous (TiO2-SiO2-TeO2)/Al2O3/TiO2 composite nanostructures on glass with enhanced photocatalysis fabricated by anodization and sol-gel process. *J. Phys. Chem. B* **2003**, *107* (27), 6586–6589.

(3) (a) Varghese, O. K.; Paulose, M.; Shankar, K.; Mor, G. K.; Grimes, C. A. Water-photolysis properties of micron-length highly-ordered titania nanotube-arrays. *J. Nanosci. Nanotechnol.* **2005**, *5*(7), 1158–1165. (b) Mor, G. K.; Shankar, K.; Varghese, O. K.; Grimes, C. A. Photoelectrochemical properties of titania nanotubes. *J. Mater. Res.* **2004**, *19*(10), 2989–2996.

(4) (a) Uchida, S.; Chiba, R.; Tomiha, M.; Masaki, N.; Shirai, M. Application of titania nanotubes to a dye-sensitized solar cell. *Electrochemistry* **2002**, *70*(6), 418–420. (b) Adachi, M.; Murata, Y.; Okada, I.; Yoshikawa, S. Formation of titania nanotubes and applications for dye-sensitized solar cells. *J. Electrochem. Soc.* **2003**, *150*(8), G488–G493. (c) Foong, T. R. B.; Shen, Y. D.; Hu, X.; Sellinger, A. Template-Directed Liquid ALD Growth of TiO2 Nanotube Arrays: Properties and Potential in Photovoltaic Devices. *Adv. Funct. Mater.* **2010**, *20*(9), 1390–1396. (d) Yang, D. J.; Park, H.; Cho, S. J.; Kim, H. G.; Choi, W. Y. TiO2-nanotube-based dye-sensitized solar cells fabricated by an efficient anodic oxidation for high surface area. *J. Phys. Chem. Solids* **2008**, *69*(5−6), 1272–1275. (e) Yu, B. Y.; Tsai, A.; Tsai, S. P.; Wong, K. T.; Yang, Y.; Chu, C. W.; Shyue, J. J., Efficient inverted solar cells using TiO2 nanotube arrays. *Nanotechnology* **2008**, *19* (25), -; (f) Shankar, K.; Mor, G. K.; Paulose, M.; Varghese, O. K.; Grimes, C. A. Effect of device geometry on the performance of TiO2 nanotube array-organic semiconductor double heterojunction solar cells. *J. Non-Cryst. Solids* **2008**, *354*(19−25), 2767–2771.

(5) Gong, D.; Grimes, C. A.; Varghese, O. K.; Hu, W. C.; Singh, R. S.; Chen, Z.; Dickey, E. C. Titanium oxide nanotube arrays prepared by anodic oxidation. *J. Mater. Res.* **2001**, *16*(12), 3331–3334.

(6) Shankar, K.; Mor, G. K.; Prakasam, H. E.; Yoriya, S.; Paulose, M.; Varghese, O. K.; Grimes, C. A. Highly-ordered TiO2 nanotube arrays up to 220 mu m in length: use in water photoelectrolysis and dye-sensitized solar cells. *Nanotechnology* **2007**, *18*(6), 3953–3957.

(7) Mor, G. K.; Varghese, O. K.; Paulose, M.; Shankar, K.; Grimes, C. A. A review on highly ordered, vertically oriented TiO2 nanotube arrays: Fabrication, material properties, and solar energy applications. *Sol. Energy Mater. Sol. Cells* **2006**, *90*(14), 2011–2075.

Published on Web 12/22/2010

cells.[10] Besides, hybrid devices as well as solid state dye sensitized solar cells can be realized.[11] Structures on conducting glass substrates allow frontside illumination, i.e. illumination from the substrate side, resulting in reduced loss of incident light intensity compared to cells fabricated from foils.[6,12]

Here we report on anodized Ti thin films on indium−tin oxide (ITO) coated glass substrates. The Ti serves as feed substrate for the formation of highly regular TiO_2 nanotubes. Anodizations are carried out in NH_4F-containing ethylene glycol baths. We introduce a sputtered compact TiO_2 layer underneath the Ti. This compact TiO_2 is applicable as hole-blocking layer and allows the fabrication of photovoltaic cells with selective external contacts and is commonly used in inverted organic solar cells.[13] Additionally, the TiO_2 layer protects the ITO from corrosion during the anodization process to maintain its conductivity.

The anodization process is analyzed in detail and different phases of the anodization − visible in the current−time anodization plot − can be identified. This allows controlled anodization and simplifies data analysis if new anodization parameters are applied. The influence of anodization bath temperature and anodization voltage are examined, and tubes of different length are grown using different Ti thicknesses.

In the last section, hybrid TiO_2-dye-P3HT solar cells are fabricated to investigate the advantages of nanotubular structures with high surface area in comparison with flat bilayer solar cells.

Experimental Section

All solvents were purchased from Sigma Aldrich at high purity grade. P3HT was purchased from Merck Chemicals.

Ti Anodization. ITO covered glass substrates (Kintech; 10 Ω/□) were cleaned with commercial dishwashing detergent using an ultrasonic toothbrush. Subsequently, ITOs were ultrasonicated for 15 min each in acetone and 2-propanol, rinsed with ethanol, and dried in a nitrogen stream. Prior to loading the sputter system, a 7 min oxygen plasma cleaning was performed. Approximately 50 nm of TiO_2 as a blocking layer and 0.2 μm−2 μm of Ti were DC sputtered at 500 °C with a Surrey NanoSystems Gamma 1000C sputter system at Ar pressures of 5 mTorr and 4 mTorr, respectively. Subsequently, the substrates were allowed to slowly cool down in high vacuum. Anodization was carried out using a two electrode setup with a Pt counter electrode in an ethylene glycol bath containing 0.4 wt % NH_4F (Sigma Aldrich). No water was added but the solution was stirred for at least 1 h in ambient air prior to anodization so the solution might contain some water. Samples were anodized at different temperatures between 273 and 338 K, varying anodization voltages between 10 and 25 V and for different times between 1 min and 2 h. If not otherwise noted anodizations were carried out at room temperature on 400 nm Ti samples. After anodization the samples were rinsed with water and ethanol and dried in air. A heat curing was performed at 450 °C for 1 h with heating and cooling rates of 3 °C/min in ambient atmosphere.

XRD Characterization. X-ray diffraction (XRD) analysis was performed with a Bruker D8 Diffractometer with Cu Kα radation at 40 kV and 40 mA. Start and end angles were 20° and 70°, respectively, with an increment of 0.05° and a scanning speed of 3 s per step.

SEM Imaging. For scanning electron microscopy (SEM) cross-sectional view samples were scratched with a diamond glass cutting pen, cooled in liquid nitrogen, and cleaved. Approximately 2 nm Au were sputtered on all SEM samples to avoid charging effects.

Solar Cell Production. Solar cells were produced from TiO_2 flat layers and samples with 400 nm Ti anodized at 15 V vs a Pt electrode. TiO_2 flat layers of approximately 50 nm were DC sputtered at 500 °C onto ITO substrates precleaned as described above. Both, TiO_2 flat layers and nanotubes were heat treated at 450 °C for 1 h with heating and cooling rates of 3 °C/min in ambient atmosphere. Subsequently, the samples were sensitized with the ruthenium dye Z907[14] by immersion in a 4 mM dye bath in ethanol for 18 h. Prior to P3HT deposition samples were rinsed with ethanol and dried in a nitrogen stream. P3HT solutions were prepared at concentrations of 30 mg/mL in chlorobenzene and stirred at room temperature for 18 h. For P3HT filling, the nanotube samples were put in a vacuum chamber, P3HT was drop-cast and left on the substrate for 4 min. Subsequently, the still wet sample was spincoated at 800 rpm. Bilayer devices were directly spincoated without using a vacuum process. An approximately 50 nm thick layer of poly(3,4-ethylenedioxythiophene)−polystyrenesulfonic acid (PEDOT:PSS) was spray-deposited onto the P3HT as described previously.[15] PEDOT:PSS (H.C. Starck) was used as received and diluted 1:10 in isopropanol and spincoated at 1000 rpm after spray-deposition. 100 nm of Ag were sputtered through a shadow

(8) Paulose, M.; Prakasam, H. E.; Varghese, O. K.; Peng, L.; Popat, K. C.; Mor, G. K.; Desai, T. A.; Grimes, C. A. TiO2 nanotube arrays of 1000 mu m length by anodization of titanium foil: Phenol red diffusion. *J. Phys. Chem. C* **2007**, *111*(41), 14992–14997.
(9) (a) Sadek, A. Z.; Zheng, H. D.; Latham, K.; Wlodarski, W.; Kalantar-Zadeh, K. Anodization of Ti Thin Film Deposited on ITO. *Langmuir* **2009**, *25*(1), 509–514. (b) Yu, X. F.; Li, Y. X.; Ge, W. Y.; Yang, Q. B.; Zhu, N. F.; Kalantar-Zadeh, K. Formation of nanoporous titanium oxide films on silicon substrates using an anodization process. *Nanotechnology* **2006**, *17*(3), 808–814.
(10) (a) Blom, P. W. M.; Mihailetchi, V. D.; Koster, L. J. A.; Markov, D. E. Device physics of polymer: fullerene bulk heterojunction solar cells. *Adv. Mater.* **2007**, *19*(12), 1551–1566. (b) Dennler, G.; Scharber, M. C.; Brabec, C. J. Polymer-Fullerene Bulk-Heterojunction Solar Cells. *Adv. Mater.* **2009**, *21*(13), 1323–1338. (c) Hoppe, H.; Sariciftci, N. S. Polymer Solar Cells. *Adv. Polym. Sci.* **2008**, *214*, 1–86.
(11) (a) Mor, G. K.; Shankar, K.; Paulose, M.; Varghese, O. K.; Grimes, C. A. High efficiency double heterojunction polymer photovoltaic cells using highly ordered TiO2 nanotube arrays. *Appl. Phys. Lett.* **2007**, *91* (15), -; (b) Varghese, O. K.; Paulose, M.; Grimes, C. A. Long vertically aligned titania nanotubes on transparent conducting oxide for highly efficient solar cells. *Nat. Nanotechnol.* **2009**, *4*(9), 592–597.
(12) (a) Ito, S.; Ha, N. L. C.; Rothenberger, G.; Liska, P.; Comte, P.; Zakeeruddin, S. M.; Pechy, P.; Nazeeruddin, M. K.; Gratzel, M. High-efficiency (7.2%) flexible dye-sensitized solar cells with Ti-metal substrate for nanocrystalline-TiO2 photoanode. *Chem. Commun.* **2006**, No. 38, 4004–4006. (b) Chen, C. C.; Chung, H. W.; Chen, C. H.; Lu, H. P.; Lan, C. M.; Chen, S. F.; Luo, L.; Hung, C. S.; Diau, E. W. G. Fabrication and Characterization of Anodic Titanium Oxide Nanotube Arrays of Controlled Length for Highly Efficient Dye-Sensitized Solar Cells. *J. Phys. Chem. C* **2008**, *112*(48), 19151–19157.
(13) Waldauf, C.; Morana, M.; Denk, P.; Schilinsky, P.; Coakley, K.; Choulis, S. A.; Brabec, C. J. Highly efficient inverted organic photovoltaics using solution based titanium oxide as electron selective contact. *Appl. Phys. Lett.* **2006**, *89*(23), 233517.
(14) Schmidt-Mende, L.; Zakeeruddin, S. M.; Gratzel, M. Efficiency improvement in solid-state-dye-sensitized photovoltaics with an amphiphilic Ruthenium-dye. *Appl. Phys. Lett.* **2005**, *86*(1), 013504.
(15) Weickert, J.; Sun, H.; Palumbiny, C.; Hesse, H.; Schmidt-Mende, L., Spray-deposited PEDOT: PSS for inverted organic solar cells. *Sol. Energy Mater. Sol. Cells* **2010**.

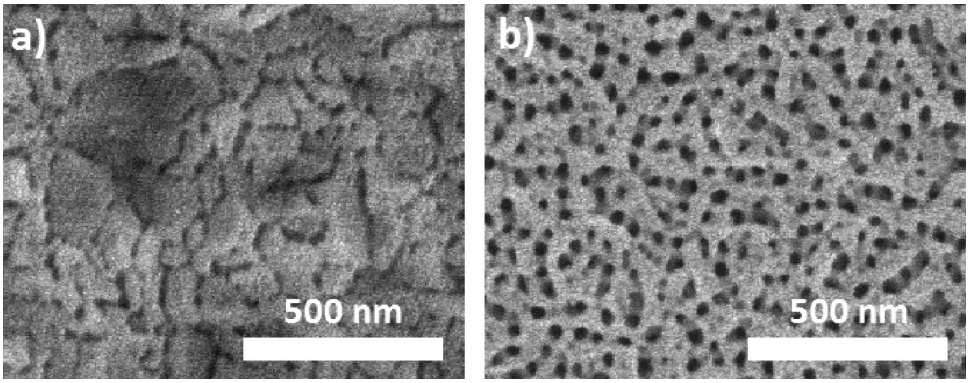

Figure 1. SEM top views of anodized Ti after **a**) 1 min and **b**) 11 min of anodization. Scale bars are 500 nm.

mask as top contacts. Finally, the fully assembled solar cells were annealed at 140 °C for 10 min in ambient air.

Solar Cell Characterization. Photovoltaic devices were tested under simulated solar light using a solar simulator with a Xe-lamp and AM 1.5G filters. Light intensity was adjusted to 100 mW/cm^2 using a Fraunhofer Institute certified Si reference cell with a KG 5 filter. For EQE measurements a 150 W xenon lamp in combination with an Omni150 (LOT-Oriel) monochromator (incident power at 490 nm ~0.3 mW/cm^2) was used. Current−voltage characteristics and external quantum efficiencies (EQE) were recorded with a Keithley Sourcemeter 2400 using a self-written LabView program.

Results and Discussion

TiO_2 Crystallinity. X-ray diffraction measurements reveal anatase TiO_2 structure after the 450 °C heat treatment (not shown). This is in good accordance with literature.[16]

Anodization Process. To gain a better understanding of the time vs current anodization curve and the time evolution of the anodization process, anodization was stopped after different times, and samples were analyzed in the SEM. Anodization was carried out at 20 V vs Pt electrode and room temperature for this experiment. Figure 1 shows an SEM top view image of a Ti film after anodization for 1 and 11 min. In the beginning pore formation occurs mainly at the Ti grain boundaries. However, after a few minutes not all pores are evolving further, and the pores are distributed more homogenously over the substrate.

Note that top view images show rather a porous instead of a tubular structure, whereas cross-sectional views clearly reveal the presence of TiO_2 nanotubes. A thin layer is forming on top of the anodized sample similar to the barrier layer reported by Sadek et al.[9a] This is discussed later in detail.

Figure 2 shows SEM cross-sectional views for increasing anodization times. Respective anodization current vs time plots are given in the insets. The series reveals an anodization mechanism similar to the one proposed by Mor et al.[7] for anodization of Ti foils. During the first seconds the Ti is anodized (i.e., oxidized) at the top and a compact TiO_2 barrier layer is formed (Figure 2a) following the equation

$$Ti \rightarrow Ti^{4+} + 4e^-$$

Small cracks, grain boundaries, and surface roughness then probably lead to field-enhanced dissolution of the TiO_2 similar to the mechanism for anodized alumina membranes.[17] Dissolution of TiO_2 is supposed to follow the equation proposed by Mor et al.[18]

$$Ti^{4+}{}_{(s)} + 6F^-{}_{(aq)} \rightarrow [TiF_6]^{2-}{}_{(aq)}$$

After two minutes (Figure 2b) the TiO_2 barrier layer has moved deeper inside the substrates and tubes have formed on top. While the tubes grow longer (Figure 2c) the thickness of the barrier layer is maintained at around 100 nm. The relatively thick barrier layer might be the reason why anodization of extremely thin Ti films of 100−200 nm does not lead to regular tubular structures but rather to porous TiO_2.[4e,9b]

After anodization for 9 min the anodization current starts to drop as the barrier layer gets thinner and only little Ti is left for anodization (Figure 2d). After 11 min the anodization current is at a local minimum with no Ti being left for oxidation (Figure 2e). However, field enhanced dissolution of the TiO_2 still occurs, and tubes are forming down to the compact TiO_2 layer that is sputtered underneath the Ti. Subsequently, also this TiO_2 compact layer gets dissolved. Accordingly, the ITO is exposed to the anodization bath. A second peak in anodization current appears which is attributed to the anodization of ITO. Figure 2f reveals that after 21 min of anodization the ITO is completely corroded by the NH_4F, whereas the tubular structure is maintained and not affected by the fluoride ions. Our experiments show that exposure of the

(16) (a) Mor, G. K.; Varghese, O. K.; Paulose, M.; Grimes, C. A. Transparent highly ordered TiO2 nanotube arrays via anodization of titanium thin films. *Adv Funct Mater* **2005**, *15*(8), 1291–1296. (b) Macak, J. M.; Tsuchiya, H.; Ghicov, A.; Schmuki, P. Dye-sensitized anodic TiO2 nanotubes. *Electrochem. Commun.* **2005**, *7*(11), 1133–1137. (c) Macak, J. M.; Zlamal, M.; Krysa, J.; Schmuki, P. Self-organized TiO2 nanotube layers as highly efficient photocatalysts. *Small* **2007**, *3*(2), 300–304.

(17) Musselman, K. P.; Mulholland, G. J.; Robinson, A. P.; Schmidt-Mende, L.; MacManus-Driscoll, J. L. Low-Temperature Synthesis of Large-Area, Free-Standing Nanorod Arrays on ITO/Glass and other Conducting Substrates. *Adv. Mater.* **2008**, *20*(23), 4470–4475.

(18) Mor, G. K.; Varghese, O. K.; Paulose, M.; Mukherjee, N.; Grimes, C. A. Fabrication of tapered, conical-shaped titania nanotubes. *J. Mater. Res.* **2003**, *18*(11), 2588–2593.

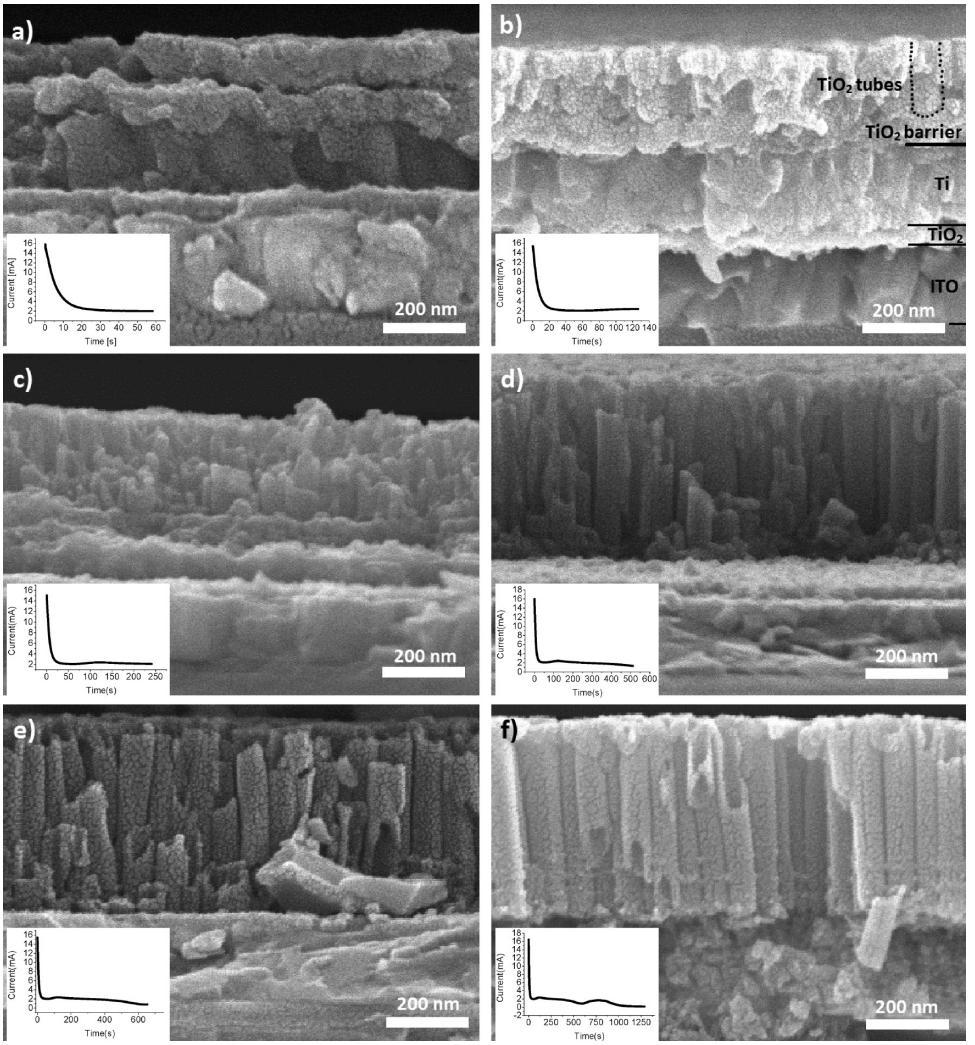

Figure 2. SEM cross-sectional views of anodized Ti after anodization for a) 1 min, b) 2 min, c) 4 min, d) 9 min, e) 11 min, and f) 21 min at room temperature and 20 V vs Pt electrode. Scale bars correspond to 200 nm. The small dots are sputtered gold particles and might not be confused with morphological features of the TiO_2. Anodization current vs time plots are given in the insets.

structures to NH_4F for 1 h without applied voltage does not significantly corrode the TiO_2.

As mentioned above a barrier layer is formed on top of the structures. The tubes clog over a thickness of approximately 30−50 nm where only the tube interiors (referred to as pores) are exposed to the top, whereas the voids between the tubes are closed.

Figure 3 shows a detailed plot of anodization current vs time for the 21 min anodized Ti. Different phases of the anodization process which could be identified from the SEM analysis (Figure 2) are also reflected in the current response.

During the first seconds a high anodization current is detected when the Ti at the surface is oxidized. The current quickly drops to a local minimum once the barrier layer is completely formed (1). The oxidation of Ti temporarily slows down before first pores are forming due to field enhancement effects. The current peaks once all tubes are regularly formed (2) and slightly decreases during the next minutes where the tubes grow deeper inside the substrate (3). In this phase of the anodization the Ti oxidation and accordingly the anodization current

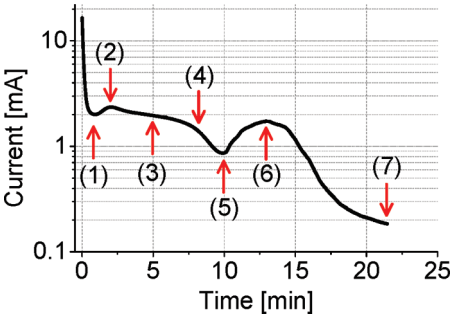

Figure 3. Current vs time plot for a long time anodization at 20 V vs Pt electrode. (1−7) label different phases of the anodization process as discussed in the text.

are limited by the field enhanced dissolution of TiO_2. The slightly decreasing current might be related to diffusion of fluoride ions into the tubes which takes longer for elongated tubes.

The following significant current drop (4) is attributed to a complete consumption of Ti, first locally and finally over the whole substrate. At this point the current reaches a local minimum (5).

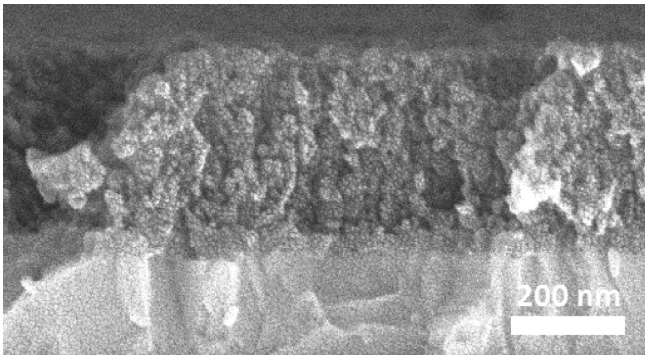

Figure 4. SEM cross-sectional view of Ti anodized at 273 K. Scale bar is 200 nm.

Table 1. Pore-Pore Distance, Pore Diameter, and Tube Wall Thickness for Anodization Temperatures Ranging from 273 to 338 K

anodization temperature [K]	pore-pore distance [nm]	pore diameter [nm]	tube wall thickness [nm]
273	34.6 ± 8.1	20 ± 3.2	N/A
298	37.1 ± 5.1	23.9 ± 1.9	13.8 ± 1.4
308	42.8 ± 5.3	23.6 ± 2.5	11.2 ± 1.2
318	44.7 ± 5.5	26 ± 3.5	9.4 ± 1.2
328	40.4 ± 5.3	28.6 ± 4.2	8.5 ± 2.0
338	41.1 ± 3.3	25.2 ± 3.1	8 ± 1.7

Once tubes have emerged also through the compact TiO_2 layer, the ITO gets anodized resulting in a second anodization peak (6). After complete corrosion of the ITO the current drops to an overall minimum (7), and no further current features are detected if the anodization is carried out for an additional hour (not shown).

We note that although formation of a TiO_2 barrier layer and growth of tubes are clearly visible from our data, it is impossible to infer whether tube forming occurs due to parallel formation of pores and voids as suggested by Mor et al.[7] or because of tube separation as described by Raja et al.[19]

Anodization Temperature. In a second experiment we investigate the influence of anodization bath temperature on structure and shape of the resulting nanostructures. Anodization was carried out at 20 V vs Pt electrode at temperatures ranging from 273 to 338 K.

A less regular structure is forming if the anodization is carried out at 273 K. Figure 4 shows an SEM cross-sectional view of the respective sample revealing tube-like but highly corroded structures. Apparently, TiO_2 is also unselectively, i.e. not due to field enhancement effects, dissolved leading to an eroded structure. Additionally, the tube length is smaller than 400 nm − the thickness of the initial Ti substrate − which is a further hint for unselective dissolution of TiO_2. Usually, the resulting TiO_2 structures are about 20−30% thicker than the feed substrate.

TiO_2 nanotubes of very similar shape and structure are obtained between 298 and 338 K. No significant differences are found in pore diameter and pore−pore distance

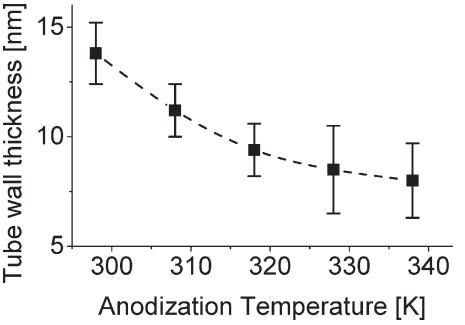

Figure 5. Tube wall thickness depending on the anodization temperature. Mean values and error bars are gained from analyzing SEM side view images. The dashed line is a guide to the eye.

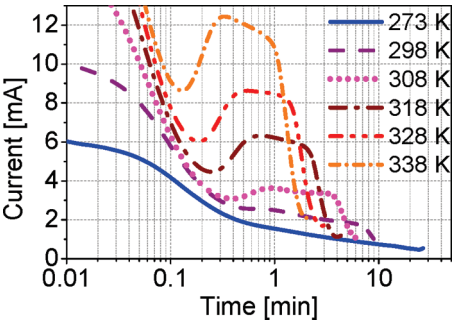

Figure 6. Anodization current vs time plots for different anodization bath temperatures.

(see Table 1). However, the tube wall thickness is significantly affected by the anodization temperature. This is in good accordance with results reported for anodization of Ti foils.[20]

Figure 5 shows a plot of tube wall thickness vs anodization temperature with the 273 K data point left out since it is not possible to obtain reliable values from the SEM analysis of the corroded structure. Thickness of the tube walls decreases significantly with increasing anodization bath temperature. For the investigated temperature range the dependence is neither clearly linear nor exponential.

In addition to different tube wall thicknesses, the shape of the anodization curves is significantly altered for increasing anodization temperatures. Figure 6 shows current vs time plots for anodization temperatures between 273 and 338 K. Except for the 273 K anodization all curves show a local current minimum after the first quick current drop. Additionally, the slope of the current drop is steeper at higher temperatures and becomes almost similar for temperatures above 308 K, suggesting that the first step − the formation of the barrier layer − is less diffusion limited than the tube formation. However, at low temperature and room temperature the transport of O^{2-} ions toward the anodized Ti might be relatively slower due to the high viscosity of the ethylene glycol causing a slower oxidation of the Ti.

The local maximum after the initial current is more pronounced for increasing temperature. This is attributed

(19) Raja, K. S.; Misra, M.; Paramguru, K. Formation of self-ordered nano-tubular structure of anodic oxide layer on titanium. *Electrochim. Acta* **2005**, *51*(1), 154–165.

(20) Mor, G. K.; Shankar, K.; Paulose, M.; Varghese, O. K.; Grimes, C. A. Enhanced photocleavage of water using titania nanotube arrays. *Nano Lett.* **2005**, *5*(1), 191–195.

Table 2. Pore-Pore Distance, Pore Diameter, and Tube Wall Thickness for Different Anodization Voltages

anodization voltage [V]	pore-pore distance [nm]	pore diameter [nm]	tube wall thickness [nm]
10	29.1 ± 4.0	17.1 ± 2.9	6.8 ± 0.9
15	38.3 ± 4.0	21.2 ± 2.9	10.5 ± 2.4
20	51.6 ± 5.5	28.3 ± 4.8	13.8 ± 1.4
25	63.0 ± 9.8	34.7 ± 3.4	14.7 ± 2.4

to a much quicker tube formation and accordingly a faster oxidation of new Ti underneath the TiO_2 barrier layer. This is consistent with overall shorter anodization times for higher temperatures. At 338 K it takes only about 1 min to anodize the 400 nm of Ti. This corresponds to a growth velocity of 24 μm/h which is even faster than values reported for tube growth in Ti foils.[6]

Anodization Voltage. Ti films were anodized at different voltages to investigate the influence of this anodization parameter. Andozations were carried out at room temperature.

Table 2 summarizes pore−pore distances, pore diameters and tube wall thicknesses found for different anodization voltages. The data are plotted in Figure 7. A linear dependence on the anodization voltage

$$D = a \cdot V_{\text{anodization}} + b$$

is found in each case where D denotes the respective dimension (pore−pore distance, pore diameter or tube wall thickness), a is the rate, and b is an intercept. Fitting parameters a and b are summarized in Table 3.

Figure 8a-d shows SEM cross-sectional views of samples anodized at 10 V, 15 V, 20, and 25 V, respectively. Highly regular structures of approximately 550 nm length are obtained for 20 and 25 V. However, at 15 V tubular structures are slightly corroded, and the effect is even stronger at 10 V. Additionally, structure length is significantly reduced after anodization at 15 and 10 V with tube lengths of only approximately 350 and 300 nm, respectively. This is attributed to less selective (i.e., field enhanced) TiO_2 etching due to the lower electric field. Besides, the anodization takes less than 5 min at 25 V but more than 20 min at 10 V. Accordingly, the TiO_2 is exposed to the fluoride ions for an elongated time at lower anodization voltages. This combination might reduce the tube lengths and erode the structure.

Anodization at low voltages also influences the surface morphology of the nanotubes. Figure 8e,f shows SEM top views of Ti films anodized at 15 and 25 V, respectively. At 25 V only pores are visible from the top since the tubes clog together at the upper ends forming a barrier layer as discussed above. In contrast, if the anodization is carried out at 10 or 15 V tubular structures can be identified even from top views.

Since the tubes are even more clearly separated from each other if films of 1 or 2 μm are anodized − meaning an overall longer anodization time (not shown) − we suppose that the barrier layer caused by the clogging tubes is etched away if the anodization is carried out for sufficient

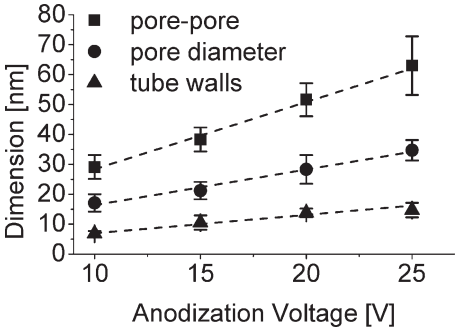

Figure 7. Pore-pore distance, pore diameter, and tube wall thickness at different anodization voltages. Dashed lines represent linear fits to the data.

Table 3. Parameters of Linear Fits ($Y = a \cdot V + b$) for Different Anodization Voltages

	a [nm/V]	b [nm]
pore-pore distance	2.2	5.9
pore diameter	1.2	4.5
tube wall thickness	0.6	0.8

times. Exposure of the structures to fluoride ions without applied electric field, however, does not result in corroded structures even after 2 h in a NH_4F bath.

We note that although highly regular tubes are not obtained at low anodization voltages the resulting structures might be particularly interesting for hybrid solar cells. The corroded TiO_2 tubes should provide a large area but still perfectly connected charge carrier percolation pathways − both being a prerequisite for efficient organic and hybrid solar cells.[21]

Tube Length. We also anodized Ti layers of varying thicknesses. For thicknesses below 200 nm no regular tubular structures but more porous films are obtained. For Ti layers of 400 nm to 2 μm similar structures of different length are found. Figure 9 shows SEM images of 2 μm Ti anodized at 20 V. As mentioned above the top view reveals tubes rather than pores after the relatively long anodization. Exposure of the top barrier layer to the fluoride ions for a relatively long time during the anodization process and the continuous presence of an electric field seem to remove the barrier layer and leave the tubes more separated from each other.

Experiments reveal that structures of different length can be easily obtained by varying the thickness of the Ti feed substrate.

Photovoltaic Devices. We fabricated TiO_2-dye-P3HT solar cells to test the application of our nanotubes in hybrid photovoltaics. Solar cells were built from 400 nm Ti films anodized at 15 V and on flat compact TiO_2 layers similar to the blocking layer which is sputtered underneath the nanotubes. Anodizations of the nanostructured devices were stopped between points (4) and (5) of the anodization curve (see Figure 3) to maintain a compact hole blocking TiO_2 layer and make the bottom electrode electron selective.

(21) Hoppe, H.; Sariciftci, N. S. Organic solar cells: An overview. *J. Mater. Res.* **2004**, *19*(7), 1924–1945.

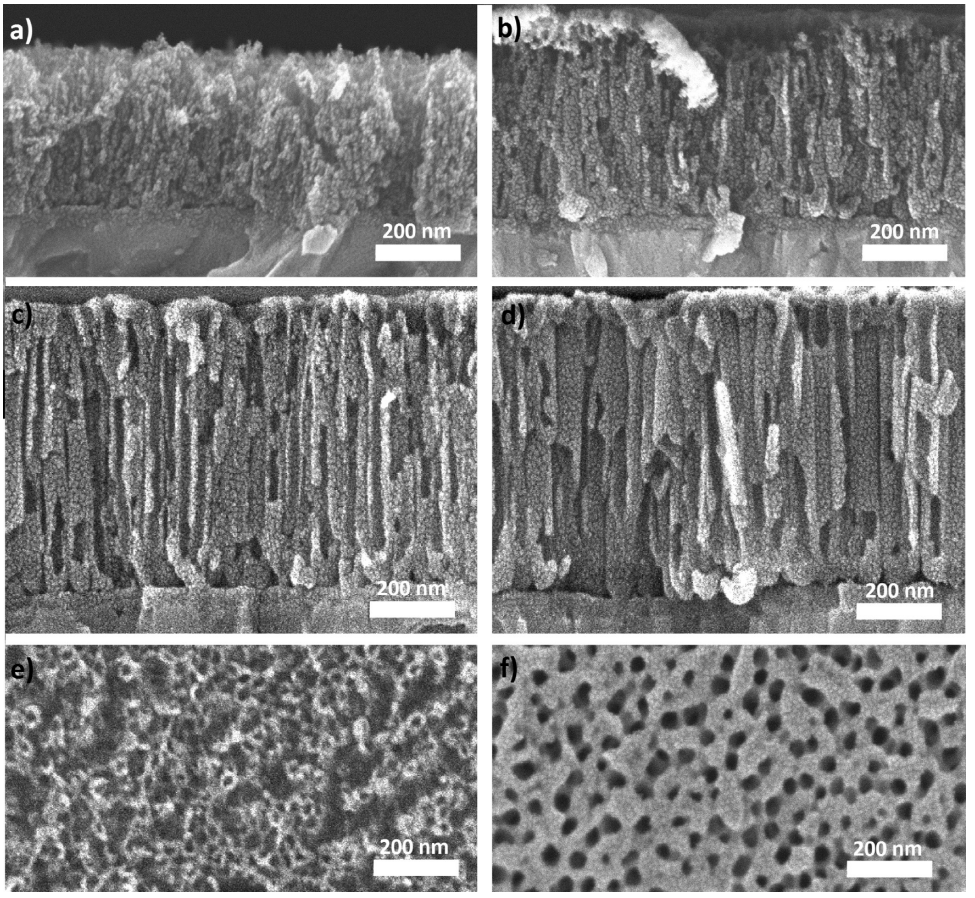

Figure 8. SEM cross-sectional view of Ti anodized at a) 10 V, b) 15 V, c) 20 V, and d) 25 V vs Pt. e) and f) show SEM top views of a 15 V and a 25 V sample, respectively. Scalebars correspond to 200 nm.

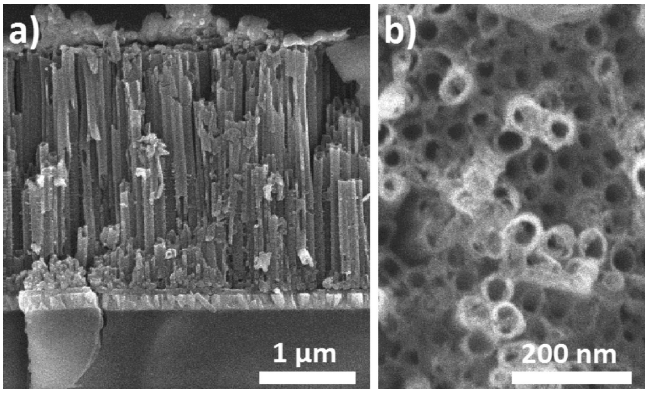

Figure 9. SEM images of 2 μm Ti anodized at 20 V vs Pt. a) cross-sectional view (scale bar 1 μm), b) top view (scale bar 200 nm).

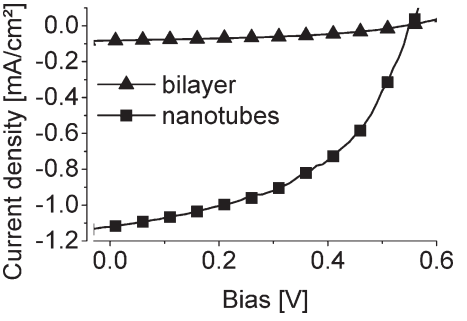

Figure 10. Current−voltage characteristics for TiO_2−P3HT hybrid solar cells. Data are shown for a bilayered device with flat TiO_2 (triangles) and for a device with nanotubes anodized at 15 V (squares).

Figure 10 shows current−voltage characteristics of typical cells recorded under illumination with simulated solar light. Similar open circuit voltages (V_{OC}) around 550 mV are detected for both cell types, but large variations are found in power conversion efficiency (PCE) and short circuit current density (I_{SC}). PCE values of 0.02% and 0.3% and I_{SC} of 0.1 mA/cm^2 and 1.1 mA/cm^2 are obtained for bilayered and nanostructured devices, rexspectively. Similar trends are found in external quantum efficiencies (EQE) which are around 1.5% and 10% for bilayer and nanostructure, respectively (not shown). EQE data also reveal that current is generated not only from exciting the dye but also from excitation of the P3HT.

The significantly improved performance of the nanostructured device is attributed to a larger donor−acceptor interface leading to enhanced charge separation and higher photocurrents. Besides, the comparable V_{OC} values for the two devices suggest that recombination losses are not significantly limiting the performance for the nanostructured device.

The overall very low efficiencies are attributed to nonoptimized fabrication methods and incomplete filling with P3HT. Besides, the energy levels of the Z907 dye are

supposed to be nonideal for the combination with P3HT since the dye has a slightly higher lowest unoccupied molecular orbital (LUMO) and a slightly lower highest occupied molecular orbital (HOMO). Further improvements in device performance could probably be gained after a $TiCl_4$ treatment for the nanostructures,[22] by using a dye with an absorption complementary to P3HT[23] or via treatments with lithium salts and 4-tert-butylpyridine.[24] Nevertheless, direct comparison of bilayered and nanostructured geometry reveals the high potential of the nanotubes for applications in hybrid photovoltaic.

Conclusion

Ti sputtering onto conducting glass substrates and subsequent anodization in NH_4F-containing ethylene glycol bath allows the controlled fabrication of ordered and highly regular TiO_2 nanotubes. By detailed analysis of anodization curves and SEM images the anodization process of TiO_2 is better understood and can be easier controlled. Structure length, pore−pore distance, pore diameter, and tube wall thickness can be controlled via Ti thickness, electric field, and anodization temperature. The obtained tubular structures on top of a compact TiO_2 layer on conducting glass facilitate the fabrication of solid state hybrid solar cells that can be illuminated from the substrate side whereas anodization of Ti foils always requires backside illumination. The presented structures offer the potential to fabricate high efficiency TiO_2-dye-P3HT solar cells as well as extremely thin absorber devices and solid state dye-sensitized solar cells with adjustable TiO_2 dimensions. Experiments show a large improvement for P3HT hybrid devices if TiO_2 nanotubes are used instead of flat TiO_2 layers with significant improvements of I_{SC} and PCE.

Acknowledgment. We acknowledge supported by the German Excellence Initiative of the Deutsche Forschungsgemeinschaft (DFG) via the "Nanosystems Initiative Munich (NIM)" and the German research foundation (DFG) in the program "SPP1355: Elementary processes of organic photovoltaics".

Supporting Information Available: Figure S1. This material is available free of charge via the Internet at http://pubs.acs.org.

(22) Sommeling, P. M.; O'Regan, B. C.; Haswell, R. R.; Smit, H. J. P.; Bakker, N. J.; Smits, J. J. T.; Kroon, J. M.; van Roosmalen, J. A. M. Influence of a TiCl4 post-treatment on nanocrystalline TiO2 films in dye-sensitized solar cells. *J. Phys. Chem. B* **2006**, *110* (39), 19191–19197.

(23) Mor, G.; Kim, S.; Paulose, M.; Varghese, O.; Shankar, K.; Basham, J.; Grimes, C. Visible to Near-Infrared Light Harvesting in TiO2 Nanotube Array- P3HT Based Heterojunction Solar Cells. *Nano Lett* **2009**, *9*(12), 4250–4257.

(24) Zhu, R.; Jiang, C. Y.; Liu, B.; Ramakrishna, S. Highly Efficient Nanoporous TiO2-Polythiophene Hybrid Solar Cells Based on Interfacial Modification Using a Metal-Free Organic Dye. *Adv. Mater.* **2009**, *21*(9), 994–1000.